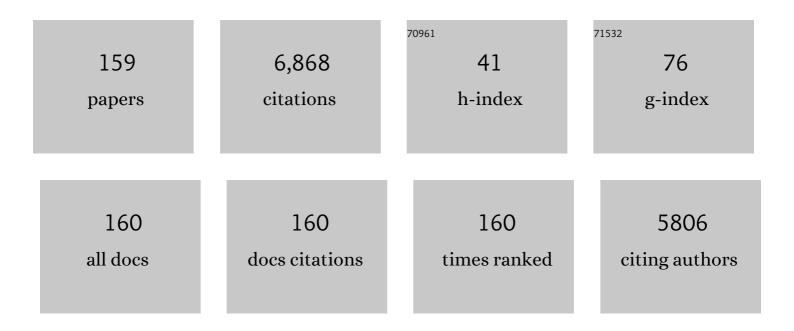
List of Publications by Year in descending order

Source: https://exaly.com/author-pdf/1766671/publications.pdf Version: 2024-02-01



LUN LANC

#	Article	IF	CITATIONS
1	Immobilization of Cu(II), Pb(II) and Cd(II) by the addition of rice straw derived biochar to a simulated polluted Ultisol. Journal of Hazardous Materials, 2012, 229-230, 145-150.	6.5	440
2	Strategies to approach high performance in Cr3+-doped phosphors for high-power NIR-LED light sources. Light: Science and Applications, 2020, 9, 86.	7.7	432
3	YAG:Ce ³⁺ Transparent Ceramic Phosphors Brighten the Nextâ€Generation Laserâ€Driven Lighting. Advanced Materials, 2020, 32, e1907888.	11.1	323
4	Adsorption of Pb(II) on variable charge soils amended with rice-straw derived biochar. Chemosphere, 2012, 89, 249-256.	4.2	295
5	pH buffering capacity of acid soils from tropical and subtropical regions of China as influenced by incorporation of crop straw biochars. Journal of Soils and Sediments, 2012, 12, 494-502.	1.5	233
6	An excellent cyan-emitting orthosilicate phosphor for NUV-pumped white LED application. Journal of Materials Chemistry C, 2017, 5, 12365-12377.	2.7	203
7	Exceptional plasticity in the bulk single-crystalline van der Waals semiconductor InSe. Science, 2020, 369, 542-545.	6.0	163
8	Ba ₉ Lu ₂ Si ₆ O ₂₄ :Ce ³⁺ : An Efficient Green Phosphor with High Thermal and Radiation Stability for Solidâ€6tate Lighting. Advanced Optical Materials, 2015, 3, 1096-1101.	3.6	160
9	Valence band engineering and thermoelectric performance optimization in SnTe by Mn-alloying via a zone-melting method. Journal of Materials Chemistry A, 2015, 3, 19974-19979.	5.2	141
10	Enhanced thermoelectric performance in p-type polycrystalline SnSe benefiting from texture modulation. Journal of Materials Chemistry C, 2016, 4, 1201-1207.	2.7	125
11	Warm White Light with a High Color-Rendering Index from a Single Gd ₃ Al ₄ GaO ₁₂ :Ce ³⁺ Transparent Ceramic for High-Power LEDs and LDs. ACS Applied Materials & Interfaces, 2019, 11, 2130-2139.	4.0	124
12	Efficient and Broadband LiGaP ₂ O ₇ :Cr ³⁺ Phosphors for Smart Nearâ€Infrared Lightâ€Emitting Diodes. Laser and Photonics Reviews, 2021, 15, 2100227.	4.4	117
13	Adsorption of Cr(III) from acidic solutions by crop straw derived biochars. Journal of Environmental Sciences, 2013, 25, 1957-1965.	3.2	113
14	Agro-C: A biogeophysical model for simulating the carbon budget of agroecosystems. Agricultural and Forest Meteorology, 2009, 149, 106-129.	1.9	110
15	Mechanisms for Increasing the pH Buffering Capacity of an Acidic Ultisol by Crop Residue-Derived Biochars. Journal of Agricultural and Food Chemistry, 2017, 65, 8111-8119.	2.4	103
16	Manipulating Band Convergence and Resonant State in Thermoelectric Material SnTe by Mn–In Codoping. ACS Energy Letters, 2017, 2, 1203-1207.	8.8	98
17	Adsorption and desorption of Cu(II) and Pb(II) in paddy soils cultivated for various years in the subtropical China. Journal of Environmental Sciences, 2010, 22, 689-695.	3.2	97
18	Application of crop straw derived biochars to Cu(II) contaminated Ultisol: Evaluating role of alkali and organic functional groups in Cu(II) immobilization. Bioresource Technology, 2013, 133, 537-545.	4.8	91

#	Article	IF	CITATIONS
19	Mobilization of phosphate in variable-charge soils amended with biochars derived from crop straws. Soil and Tillage Research, 2015, 146, 139-147.	2.6	91
20	Water-mediated cation intercalation of open-framework indium hexacyanoferrate with high voltage and fast kinetics. Nature Communications, 2016, 7, 11982.	5.8	90
21	High Efficiency Green Phosphor Ba ₉ Lu ₂ Si ₆ O ₂₄ :Tb ³⁺ : Visible Quantum Cutting via Cross-Relaxation Energy Transfers. Journal of Physical Chemistry C, 2016, 120, 2362-2370.	1.5	89
22	First-Principles Simulations of Inelastic Electron Tunneling Spectroscopy of Molecular Electronic Devices. Nano Letters, 2005, 5, 1551-1555.	4.5	87
23	Thermally Stable CaLu ₂ Mg ₂ Si ₃ O ₁₂ :Cr ³⁺ Phosphors for NIR LEDs. Advanced Optical Materials, 2021, 9, 2100388.	3.6	84
24	Removal of Cr(VI) from aqueous solutions by Na2SO3/FeSO4 combined with peanut straw biochar. Chemosphere, 2014, 101, 71-76.	4.2	83
25	Massive red-shifting of Ce ³⁺ emission by Mg ²⁺ and Si ⁴⁺ doping of YAG:Ce transparent ceramic phosphors. Journal of Materials Chemistry C, 2018, 6, 12200-12205.	2.7	82
26	Enhanced thermopower in rock-salt SnTe–CdTe from band convergence. RSC Advances, 2016, 6, 32189-32192.	1.7	72
27	Red-Emitting Phosphor Ba ₉ Lu ₂ Si ₆ O ₂₄ :Ce ³⁺ ,Mn ²⁺ with Enhanced Energy Transfer via Self-Charge Compensation. Journal of Physical Chemistry C, 2015, 119, 24558-24563.	1.5	69
28	The mechanism of chromate sorption by three variable charge soils. Chemosphere, 2008, 71, 1469-1475.	4.2	60
29	YAGC:Ce transparent ceramics with high luminous efficiency for solid-state lighting application. Journal of Advanced Ceramics, 2019, 8, 389-398.	8.9	56
30	Adsorption Properties of Subtropical and Tropical Variable Charge Soils: Implications from Climate Change and Biochar Amendment. Advances in Agronomy, 2016, 135, 1-58.	2.4	54
31	A first-principles study on the phonon transport in layered BiCuOSe. Scientific Reports, 2016, 6, 21035.	1.6	52
32	Mediating Point Defects Endows n‶ype Bi ₂ Te ₃ with High Thermoelectric Performance and Superior Mechanical Robustness for Power Generation Application. Small, 2022, 18, e2201352.	5.2	51
33	Evaluation of ferrolysis in arsenate adsorption on the paddy soil derived from an Oxisol. Chemosphere, 2017, 179, 232-241.	4.2	50
34	Enhanced thermoelectric figure of merit in p-type Bi0.48Sb1.52Te3 alloy with WSe2 addition. Journal of Materials Chemistry A, 2014, 2, 8512.	5.2	49
35	Texturing degree boosts thermoelectric performance of silver-doped polycrystalline SnSe. NPG Asia Materials, 2017, 9, e426-e426.	3.8	49
36	Broadband emissions from Lu ₂ Mg ₂ Al ₂ Si ₂ O ₁₂ :Ce ³⁺ plate ceramic phosphors enable a high color-rendering index for laser-driven lighting. Journal of Materials Chemistry C, 2020, 8, 1405-1412.	2.7	49

#	Article	IF	CITATIONS
37	Peanut straw biochar increases the resistance of two Ultisols derived from different parent materials to acidification: A mechanism study. Journal of Environmental Management, 2018, 210, 171-179.	3.8	48
38	Improving Thermoelectric Performance of αâ€MgAgSb by Theoretical Band Engineering Design. Advanced Energy Materials, 2017, 7, 1700076.	10.2	46
39	Optimizing the thermoelectric performance of In–Cd codoped SnTe by introducing Sn vacancies. Journal of Materials Chemistry C, 2017, 5, 7504-7509.	2.7	46
40	Transparent Ceramics Enabling High Luminous Flux and Efficacy for the Next-Generation High-Power LED Light. ACS Applied Materials & Interfaces, 2019, 11, 21697-21701.	4.0	45
41	Super Large Sn _{1–<i>x</i>} Se Single Crystals with Excellent Thermoelectric Performance. ACS Applied Materials & Interfaces, 2019, 11, 8051-8059.	4.0	43
42	High Efficiency Greenâ€Emitting LuAG:Ce Ceramic Phosphors for Laser Diode Lighting. Advanced Optical Materials, 2021, 9, 2002141.	3.6	43
43	Rice Straw-Derived Biochar Properties and Functions as Cu(II) and Cyromazine Sorbents as Influenced by Pyrolysis Temperature. Pedosphere, 2015, 25, 781-789.	2.1	41
44	Charge Transport in Thermoelectric SnSe Single Crystals. ACS Energy Letters, 2018, 3, 689-694.	8.8	41
45	CaAlSiN ₃ :Eu ²⁺ /Lu ₃ Al ₅ O ₁₂ :Ce ³⁺ phosphor-in-glass film with high luminous efficiency and CRI for laser diode lighting. Journal of Materials Chemistry C, 2021, 9, 3522-3530.	2.7	41
46	Origin and Luminescence of Anomalous Red-Emitting Center in Rhombohedral Ba ₉ Lu ₂ Si ₆ O ₂₄ :Eu ²⁺ Blue Phosphor. Inorganic Chemistry, 2016, 55, 8628-8635.	1.9	40
47	Enhanced thermoelectric performance in n-type polycrystalline SnSe by PbBr ₂ doping. RSC Advances, 2017, 7, 17906-17912.	1.7	40
48	Enhanced thermoelectric performance in In1â^'xGaxSb originating from the scattering of point defects and nanoinclusion. Journal of Materials Chemistry, 2011, 21, 12398.	6.7	39
49	Characteristics of biomass ashes from different materials and their ameliorative effects on acid soils. Journal of Environmental Sciences, 2017, 55, 294-302.	3.2	39
50	Incorporation of corn straw biochar inhibited the re-acidification of four acidic soils derived from different parent materials. Environmental Science and Pollution Research, 2018, 25, 9662-9672.	2.7	39
51	Mechanism of Cu(II) and Cd(II) immobilization by extracellular polymeric substances (Escherichia coli) on variable charge soils. Environmental Pollution, 2019, 247, 136-145.	3.7	39
52	Thermoelectric (Bi,Sb)2Te3–Ge0.5Mn0.5Te composites with excellent mechanical properties. Journal of Materials Chemistry A, 2019, 7, 9241-9246.	5.2	37
53	Ultralow Lattice Thermal Conductivity in SnTe by Manipulating the Electron–Phonon Coupling. Journal of Physical Chemistry C, 2019, 123, 15996-16002.	1.5	36
54	Band engineering and crystal field screening in thermoelectric Mg ₃ Sb ₂ . Journal of Materials Chemistry A, 2019, 7, 8922-8928.	5.2	36

#	Article	lF	CITATIONS
55	Bi–Zn codoping in GeTe synergistically enhances band convergence and phonon scattering for high thermoelectric performance. Journal of Materials Chemistry A, 2020, 8, 21642-21648.	5.2	36
56	The mechanisms underlying the reduction in aluminum toxicity and improvements in the yield of sweet potato (Ipomoea batatas L.) After organic and inorganic amendment of an acidic ultisol. Agriculture, Ecosystems and Environment, 2020, 288, 106716.	2.5	33
57	Fermi-surface dynamics and high thermoelectric performance along the out-of-plane direction in n-type SnSe crystals. Energy and Environmental Science, 2020, 13, 616-621.	15.6	32
58	Preparation and Optical Properties of Transparent (Ce,Gd) ₃ Al ₃ Ga ₂ O ₁₂ Ceramics. Journal of the American Ceramic Society, 2015, 98, 2352-2356.	1.9	31
59	Amelioration of soil acidity, Olsen-P, and phosphatase activity by manure- and peat-derived biochars in different acidic soils. Arabian Journal of Geosciences, 2018, 11, 1.	0.6	31
60	Investigating the thermoelectric performance of n-type SnSe: the synergistic effect of NbCl ₅ doping and dislocation engineering. Journal of Materials Chemistry C, 2020, 8, 13244-13252.	2.7	31
61	Refined band structure plus enhanced phonon scattering realizes thermoelectric performance optimization in Cul–Mn codoped SnTe. Journal of Materials Chemistry A, 2021, 9, 13065-13070.	5.2	30
62	Highâ€Performance Thermoelectric Material and Module Driven by Mediumâ€Entropy Engineering in SnTe. Advanced Functional Materials, 2022, 32, .	7.8	30
63	Synergistic Optimization of Thermoelectric Performance in P-Type Bi0.48Sb1.52Te3/Graphene Composite. Energies, 2016, 9, 236.	1.6	29
64	Study on Thermoelectric Properties of Polycrystalline SnSe by Ge Doping. Journal of Electronic Materials, 2017, 46, 3182-3186.	1.0	29
65	Enhanced thermoelectric figure of merit in p-type BiSbTeSe alloy with ZnSb addition. Journal of Materials Chemistry A, 2013, 1, 966-969.	5.2	28
66	Effect of low energy-consuming biochars in combination with nitrate fertilizer on soil acidity amelioration and maize growth. Journal of Soils and Sediments, 2017, 17, 790-799.	1.5	28
67	Critical pH and exchangeable Al of four acidic soils derived from different parent materials for maize crops. Journal of Soils and Sediments, 2018, 18, 1490-1499.	1.5	28
68	Effect of aluminum modification of rice straw–based biochar on arsenate adsorption. Journal of Soils and Sediments, 2020, 20, 3073-3082.	1.5	28
69	Surface chemical properties and pedogenesis of tropical soils derived from basalts with different ages in Hainan, China. Catena, 2011, 87, 334-340.	2.2	27
70	Effect of Yb3+ on the Crystal Structural Modification and Photoluminescence Properties of GGAG:Ce3+. Inorganic Chemistry, 2016, 55, 3040-3046.	1.9	27
71	Thermoelectric properties of textured polycrystalline Na _{0.03} Sn _{0.97} Se enhanced by hot deformation. Journal of Materials Chemistry A, 2018, 6, 23730-23735.	5.2	27
72	Comparison of the surface chemical properties of four soils derived from Quaternary red earth as related to soil evolution. Catena, 2010, 80, 154-161.	2.2	26

#	Article	IF	CITATIONS
73	Effect of Crop-Straw Derived Biochars on Pb(II) Adsorption in Two Variable Charge Soils. Journal of Integrative Agriculture, 2014, 13, 507-516.	1.7	26
74	Paddy cultivation significantly alters the forms and contents of Fe oxides in an Oxisol and increases phosphate mobility. Soil and Tillage Research, 2018, 184, 176-180.	2.6	26
75	An elongation method for first principle simulations of electronic structures and electron transport properties of finite nanostructures. Journal of Chemical Physics, 2006, 124, 214711.	1.2	25
76	Adhesion of Escherichia coli to nano-Fe/Al oxides and its effect on the surface chemical properties of Fe/Al oxides. Colloids and Surfaces B: Biointerfaces, 2013, 110, 289-295.	2.5	25
77	Alleviation of aluminum phytotoxicity by canola straw biochars varied with their cultivating soils through an investigation of wheat seedling root elongation. Chemosphere, 2019, 218, 907-914.	4.2	24
78	Thermoelectric performance of the ordered In4Se3–In composite constructed by monotectic solidification. Journal of Materials Chemistry A, 2013, 1, 8844.	5.2	23
79	Enhancement of Cd(II) adsorption by rice straw biochar through oxidant and acid modifications. Environmental Science and Pollution Research, 2021, 28, 42787-42797.	2.7	23
80	Enhanced Thermoelectric and Mechanical Performances in Sintered Bi _{0.48} Sb _{1.52} Te ₃ –AgSbSe ₂ Composite. ACS Applied Materials & Interfaces, 2021, 13, 24937-24944.	4.0	23
81	Arsenate Adsorption from Aqueous Solution onto Fe(III)-Modified Crop Straw Biochars. Environmental Engineering Science, 2015, 32, 922-929.	0.8	22
82	Effect of Ionic Strength and Mechanism of Cu(II) Adsorption by Goethite and γ-Al ₂ O ₃ . Journal of Chemical & Engineering Data, 2010, 55, 5547-5552.	1.0	21
83	Preferential adhesion of surface groups of Bacillus subtilis on gibbsite at different ionic strengths and pHs revealed by ATR-FTIR spectroscopy. Colloids and Surfaces B: Biointerfaces, 2018, 165, 83-91.	2.5	21
84	Achieving high-performance p-type SmMg ₂ Bi ₂ thermoelectric materials through band engineering and alloying effects. Journal of Materials Chemistry A, 2020, 8, 15760-15766.	5.2	21
85	Adsorption and desorption of Cu(II) and Cd(II) in the tropical soils during pedogenesis in the basalt from Hainan, China. Carbonates and Evaporites, 2010, 25, 27-34.	0.4	20
86	The hydrothermally synthesis of K ₃ AlF ₆ :Cr ³⁺ NIR phosphor and its performance optimization based on phase control. Journal of the American Ceramic Society, 2021, 104, 5235-5243.	1.9	20
87	Effect of different phosphorus sources on soybean growth and arsenic uptake under arsenic stress conditions in an acidic ultisol. Ecotoxicology and Environmental Safety, 2018, 165, 11-18.	2.9	19
88	Optimized orientation and enhanced thermoelectric performance in Sn _{0.97} Na _{0.03} Se with Te addition. Journal of Materials Chemistry C, 2019, 7, 2653-2658.	2.7	19
89	Optimized Thermoelectric Properties of Bi _{0.48} Sb _{1.52} Te ₃ through AgCuTe Doping for Low-Grade Heat Harvesting. ACS Applied Materials & Interfaces, 2021, 13, 57514-57520.	4.0	19
90	Phosphate adsorption at variable charge soil/water interfaces as influenced by ionic strength. Soil Research, 2009, 47, 529.	0.6	18

#	Article	IF	CITATIONS
91	Interactions Between <i>Escherchia coli</i> and the Colloids of Three Variable Charge Soils and Their Effects on Soil Surface Charge Properties. Geomicrobiology Journal, 2015, 32, 511-520.	1.0	18
92	Relative abundance of chemical forms of Cu(II) and Cd(II) on soybean roots as influenced by pH, cations and organic acids. Scientific Reports, 2016, 6, 36373.	1.6	18
93	Enhanced Thermoelectric Properties of p-Type Bi _{0.48} Sb _{1.52} Te ₃ /Sb ₂ Te ₃ Composite. ACS Applied Materials & Interfaces, 2020, 12, 52922-52928.	4.0	18
94	Achieving High Thermoelectric Performance of n-Type Bi ₂ Te _{2.79} Se _{0.21} Sintered Materials by Hot-Stacked Deformation. ACS Applied Materials & Interfaces, 2021, 13, 15429-15436.	4.0	18
95	Structure and thermoelectric properties of the n-type clathrate Ba8Cu5.1Ge40.2Sn0.7. Journal of Materials Chemistry A, 2015, 3, 19100-19106.	5.2	17
96	Enhanced thermoelectric performance in p-type polycrystalline SnSe by Cu doping. Journal of Materials Science: Materials in Electronics, 2018, 29, 18727-18732.	1.1	17
97	A farâ€redâ€emitting <i>(Gd,Y)₃(Ga,Al)₅O₁₂:Mn²⁺</i> ceramic phosphor with enhanced thermal stability for plant cultivation. Journal of the American Ceramic Society, 2020, 103, 5157-5168.	1.9	17
98	Improved Thermoelectric Properties of BiSbTe-AgBiSe ₂ Alloys by Suppressing Bipolar Excitation. ACS Applied Energy Materials, 2021, 4, 2944-2950.	2.5	17
99	Synthesis of Ceriumâ€Doped <scp><scp>Gd</scp></scp> ₃ (<scp><scp>Al</scp>,<scp>,<scp>Ga</scp></scp>)_{5Powder for Ceramic Scintillators with Ultrasonicâ€Assisted Chemical Coprecipitation Method. Journal of the American Ceramic Society. 2013. 96. 3038-3041.}</scp>	ub> <scp> 1.9</scp>	<scp>O</scp>
100	Competition between bacteria and phosphate for adsorption sites on gibbsite: An in-situ ATR-FTIR spectroscopic and macroscopic study. Colloids and Surfaces B: Biointerfaces, 2016, 148, 496-502.	2.5	16
101	Effects of Amorphous Al(OH) ₃ on the Desorption of Ca ²⁺ , Mg ²⁺ , and Na ⁺ from Soils and Minerals As Related to Diffuse Layer Overlapping. Journal of Chemical & Engineering Data, 2011, 56, 2536-2542.	1.0	15
102	Paddy Cultivation Significantly Alters Phosphorus Sorption Characteristics and Loss Risk in a Calcareous Paddy Soil Chronosequence. Soil Science Society of America Journal, 2019, 83, 575-583.	1.2	15
103	Effects of crop straw biochars on aluminum species in soil solution as related with the growth and yield of canola (Brassica napus L.) in an acidic Ultisol under field condition. Environmental Science and Pollution Research, 2020, 27, 30178-30189.	2.7	15
104	Effect of composition deviation on the microstructure and luminescence properties of Nd:YAG ceramics. CrystEngComm, 2014, 16, 10856-10862.	1.3	14
105	A Direct Method to Extract Transient Sub-Gap Density of State (DOS) Based on Dual Gate Pulse Spectroscopy. Scientific Reports, 2016, 6, 24096.	1.6	14
106	Thermoelectric Performance Optimization and Phase Transition of GeTe by Alloying with Orthorhombic CuSbSe ₂ . ACS Applied Energy Materials, 2021, 4, 4242-4247.	2.5	14
107	Enhanced power factor in the promising thermoelectric material SnPb _x Te prepared via zone-melting. RSC Advances, 2015, 5, 59379-59383.	1.7	13
108	Evolution of soil surface charge in a chronosequence of paddy soil derived from Alfisol. Soil and Tillage Research, 2019, 192, 144-150.	2.6	13

#	Article	IF	CITATIONS
109	Boosting the Thermoelectric Performance of PbSe from the Band Convergence Driven By Spinâ€Orbit Coupling. Advanced Energy Materials, 2022, 12, 2103287.	10.2	13
110	Adsorption of chromate on variable charge soils as influenced by ionic strength. Environmental Earth Sciences, 2012, 66, 1155-1162.	1.3	12
111	Amelioration of an acidic ultisol by straw-derived biochars combined with dicyandiamide under application of urea. Environmental Science and Pollution Research, 2017, 24, 6698-6709.	2.7	12
112	Effect of dehydrated-attapulgite nanoinclusions on the thermoelectric properties of BiSbTe alloys. RSC Advances, 2013, 3, 4951.	1.7	11
113	Highly transparent cerium doped gadolinium gallium aluminum garnet ceramic prepared with precursors fabricated by ultrasonic enhanced chemical co-precipitation. Ultrasonics Sonochemistry, 2017, 39, 792-797.	3.8	11
114	Texture Development and Grain Alignment of Hotâ€Pressed Tetradymite Bi _{0.48} Sb _{1.52} Te ₃ via Powder Molding. Energy Technology, 2019, 7, 1900814.	1.8	11
115	Effect of Ca2+ - Si4+ on Y3Al5O12:Ce ceramic phosphors for white laser-diodes lighting. Applied Physics Letters, 2021, 118, 211902.	1.5	11
116	Negative Wien Effect Measurements for Exploring Polarization Processes of Cations Interacting with Negatively Charged Soil Particles. Soil Science Society of America Journal, 2009, 73, 569-578.	1.2	10
117	The Effects of Cation Concentration in the Salt Solution on the Cerium Doped Gadolinium Gallium Aluminum Oxide Nanopowders Prepared by a Co-precipitation Method. IEEE Transactions on Nuclear Science, 2014, 61, 301-305.	1.2	10
118	Entropy Engineering Realized Ultralow Thermal Conductivity and High Seebeck Coefficient in Lead-Free SnTe. ACS Applied Energy Materials, 2021, 4, 12738-12744.	2.5	10
119	Nano-scaled top-down of bismuth chalcogenides based on electrochemical lithium intercalation. Journal of Nanoparticle Research, 2011, 13, 6569-6578.	0.8	9
120	YAG phosphor with spatially separated luminescence centers. Journal of Materials Chemistry C, 2016, 4, 244-247.	2.7	9
121	Stabilization of Thermoelectric Properties of the Cu/Bi0.48Sb1.52Te3 Composite for Advantageous Power Generation. Journal of Electronic Materials, 2017, 46, 2746-2751.	1.0	9
122	Investigation on structure and thermoelectric properties in p-type Bi0.48Sb1.52Te3 via PbTe incorporating. Journal of Materials Science: Materials in Electronics, 2018, 29, 7701-7706.	1.1	9
123	Biochars derived from crop straws increased the availability of applied phosphorus fertilizer for maize in Ultisol and Oxisol. Environmental Science and Pollution Research, 2020, 27, 5511-5522.	2.7	9
124	Characteristics of crop straw-decayed products and their ameliorating effects on an acidic Ultisol. Archives of Agronomy and Soil Science, 2021, 67, 1708-1721.	1.3	9
125	A high-efficiency GeTe-based thermoelectric module for low-grade heat recovery. Journal of Materials Chemistry A, 2022, 10, 7677-7683.	5.2	9
126	Synergistically Optimized Thermal Conductivity and Carrier Concentration in GeTe by Bi–Se Codoping. ACS Applied Materials & Interfaces, 2022, 14, 14359-14366.	4.0	9

#	Article	IF	CITATIONS
127	Co-Precipitation Synthesis of Gadolinium Aluminum Gallium Oxide (GAGG) via Different Precipitants. IEEE Transactions on Nuclear Science, 2014, 61, 306-311.	1.2	8
128	The amelioration effects of canola straw biochar on Ultisol acidity varied with the soil in which the feedstock crop was cultivated. Journal of Soils and Sediments, 2020, 20, 1424-1434.	1.5	8
129	Direct Quantification of Sorption Thermodynamics of Phosphate on Four Soil Colloids through Isothermal Titration Calorimetry. ACS Earth and Space Chemistry, 2021, 5, 295-304.	1.2	8
130	Elucidating the mechanisms determining the availability of phosphate by application of biochars from different parent materials. Environmental Geochemistry and Health, 2022, 44, 4191-4200.	1.8	8
131	Synergistic Manipulation of Interdependent Thermoelectric Parameters in SnTe–AgBiTe ₂ Alloys by Mn Doping. ACS Applied Materials & Interfaces, 2022, 14, 29032-29038.	4.0	8
132	Inhibiting Effect of Dicyandiamide on Soil Acidification Induced by Application of Urea or Ammonium Bicarbonate. Communications in Soil Science and Plant Analysis, 2014, 45, 1823-1830.	0.6	7
133	Thermoelectric properties of CoSb3 and CoSb3/SiC composites prepared by mechanical alloying and microwave sintering. Journal of Materials Science: Materials in Electronics, 2017, 28, 10509-10515.	1.1	7
134	Effect of ferrolysis and organic matter accumulation on chromate adsorption characteristics of an Oxisol-derived paddy soil. Science of the Total Environment, 2020, 744, 140868.	3.9	6
135	Interactions of Heavy Metal Ions with Paddy Soils as Inferred from Wien Effect Measurements in Dilute Suspensions. Pedosphere, 2006, 16, 718-725.	2.1	5
136	Full spectrum core–shell phosphors under ultraviolet excitation. Chemical Communications, 2019, 55, 12188-12191.	2.2	5
137	Understanding the Band Engineering in Mg ₂ Siâ€Based Systems from Wannierâ€Orbital Analysis. Annalen Der Physik, 2020, 532, 1900543.	0.9	5
138	Isothermal titration calorimetry as a useful tool to examine adsorption mechanisms of phosphate on gibbsite at various solution conditions. Soil Science Society of America Journal, 2020, 84, 1110-1124.	1.2	5
139	Application of measuring electrochemical characteristics on plant root surfaces in screening Al-tolerant wheat. Environmental Pollution, 2021, 281, 116993.	3.7	5
140	Inhibition of phosphate sorptions on four soil colloids by two bacteria. Environmental Pollution, 2021, 290, 118001.	3.7	5
141	Dramatically enhanced Seebeck coefficient in GeMnTe2–NaBiTe2 alloys by tuning the Spin's thermodynamic entropy. Physical Chemistry Chemical Physics, 2021, 23, 17866-17872.	1.3	5
142	Unusually high Seebeck coefficient arising from temperature-dependent carrier concentration in PbSe–AgSbSe ₂ alloys. Journal of Materials Chemistry C, 2021, 9, 17365-17370.	2.7	5
143	Optimized thermoelectric properties of Bi _{0.48} Sb _{1.52} Te ₃ /BN composites. Journal of Materials Chemistry C, 2022, 10, 3172-3177.	2.7	5
144	Origin of the unique thermoelectric transport in Mg ₃ (Sb,Bi) ₂ : absence of d-orbital bonding in crystal cohesion. Journal of Materials Chemistry A, 2022, 10, 11131-11136.	5.2	5

#	Article	IF	CITATIONS
145	<i><scp>I</scp>nâ€situ</i> <scp>ATRâ€FTIR</scp> spectroscopic investigation of desorption of phosphate from haematite by bacteria. European Journal of Soil Science, 2017, 68, 480-490.	1.8	4
146	Tunable luminescent spectra via energy transfers between different lattice sites in Ce3+, Mn2+ codoped Ba9Lu2Si6O24 phosphors for NUV-based warm white LED applications. Journal of Materials Science: Materials in Electronics, 2018, 29, 4547-4556.	1.1	4
147	Adhesion mediated transport of bacterial pathogens in saturated sands coated by phyllosilicates and Al-oxides. Colloids and Surfaces B: Biointerfaces, 2019, 181, 215-225.	2.5	4
148	Enhancing phosphorus availability in two variable charge soils by the amendments of crop straw biochars. Arabian Journal of Geosciences, 2020, 13, 1.	0.6	4
149	Anomalous Thermopower and High <i>ZT</i> in GeMnTe ₂ Driven by Spin's Thermodynamic Entropy. Research, 2021, 2021, 1949070.	2.8	4
150	Wien Effect Characterization of Interactions Between Ions and Charged Sites on Clay Surfaces of Variable-Charge Soils. Pedosphere, 2009, 19, 545-553.	2.1	3
151	Effect of Ionic Strength on Specific Adsorption of Ions by Variable Charge Soils: Experimental Testification on the Adsorption Model of Bowden et al , 2010, , 78-80.		3
152	Single Crystal Structure Study of Type I Clathrate \$\$hbox {K}_{8}hbox {Zn}_4hbox {Sn}_{42}\$\$ K 8 Zn 4 Sn 42 and \$\$hbox {K}_8hbox {In}_8hbox {Sn}_{38}\$\$ K 8 In 8 Sn 38. Journal of Electronic Materials, 2017, 46, 2765-2769.	1.0	3
153	Boosted carrier mobility and enhanced thermoelectric properties of polycrystalline Na _{0.03} Sn _{0.97} Se by liquid-phase hot deformation. Materials Advances, 2020, 1, 1092-1098.	2.6	3
154	Enhancement of the efficiency and thermal stability of the double perovskite Cs ₂ AgInCl ₆ single crystal by Sc substitution. Materials Advances, 2022, 3, 4381-4386.	2.6	3
155	Effect of tea polyphenols on copper adsorption and manganese release in two variable-charge soils. Journal of Geochemical Exploration, 2018, 190, 374-380.	1.5	2
156	Thermoelectric Properties of CdTe1â ̈́x Cl x Material Prepared by Spark Plasma Sintering Method. Journal of Electronic Materials, 2014, 43, 3087-3091.	1.0	1
157	Effect of paddy cultivation on the surface electrochemical properties of differentâ€sized particles of a Gleysol. Journal of Plant Nutrition and Soil Science, 2021, 184, 471-478.	1.1	1
158	Synergistically Optimized Thermoelectric and Mechanical Properties in p â€Type BiSbTe by a Microdroplet Deposition Technique. Energy Technology, 2021, 9, 2001024.	1.8	1
159	Influence of sampling on composite structured light pattern. , 2008, , .		0